Characteristics of Small Vortices in a Turbulent Axisymmetric Jet

Sudhaker Chhabra

Pablo Huq[1]

Ajay K. Prasad[2]
e-mail: prasad@me.udel.edu

Department of Mechanical Engineering,
University of Delaware,
Newark, DE 19716-3140

Characteristics of small vortices were studied in axisymmetric jets wherein the Kolmogorov scale was approached by progressively decreasing the Reynolds number while still maintaining turbulent flow. A periodic forcing introduced far upstream of the jet nozzle ensured that the jet was turbulent. A vortex eduction tool was developed and applied to the high-pass filtered 2D velocity field in the axial plane of a turbulent jet while varying Re between 140 and 2600. Vortex population, energy, vorticity, and rms (root-mean-square velocity fluctuations) of the high-pass filtered field were measured to elucidate vortex characteristics. The observed population of vortices decreases dramatically at the Kolmogorov scale. The observed increase in vortex population with decreasing vortex size appears to be in accord with the space-filling argument, in that the vortex population in a two-dimensional domain should grow as R^{-2}. The energy density curve obtained from vortex statistics reproduces the $-5/3$ slope for the inertial subrange, and the high-pass filtered field accounts for approximately two-thirds of the total rms.
[DOI: 10.1115/1.2173292]

Introduction

Turbulent flow is comprised of eddies, ranging in size from the Kolmogorov scale (η) at the small end of the spectrum to the integral scale (b) at the large end. In most turbulence studies, the velocity signal is acquired using pointwise techniques, such as hot-wire anemometry [1,2] or laser-Doppler anemometry [2], and the time-resolved velocity signal record is analyzed to extract its spectral content. The small probe volume in these techniques is well suited to obtain measurements at even the smallest scales in the flow. In contrast, in the current research, we determine the characteristics of small eddies in a turbulent axisymmetric jet using the particle image velocimetry (PIV) measurement technique. We use a vortex eduction tool to identify vortices in the high-pass filtered 2D velocity field of a turbulent flow and extract their statistical properties, such as population density, size, circulation, and energy. We have previously applied this tool to extract vortex statistics from velocity measurements in the axial plane of a self-similar turbulent axisymmetric jet [3]. In a subsequent paper, an improved version of the tool was used to measure the variation of circulation and vorticity within vortex cores [4]. The properties of large engulfing eddies that typically reside at the jet edge were explored in [5].

An obvious difficulty with using PIV to explore the smallest flow scales is a lack of spatial resolution; it is difficult to obtain data using PIV at scales approaching the Kolmogorov scale in typical turbulent flows. One solution is to employ techniques akin to micro-PIV, where the flow is examined at sufficiently high magnifications to resolve the smallest scales. However, instead of applying progressively larger magnifications and exploring the Kolmogorov scale in that manner, our approach is to employ successively smaller jet Reynolds numbers and increase the Kolmogorov scale to the point that it becomes visible to our recording configuration wherein the spatial resolution is unchanged throughout.

At the outset, it is useful to briefly review the characteristics of vortices of various sizes. Starting from the integral scale, successive generations of eddies may be assigned a size br^n ($n=0,1,2,\ldots$, and r is some factor smaller than unity). Space-filling considerations [6] imply that the number of eddies of a particular generation will grow as r^{-3n} in three-dimensional space; in a two-dimensional domain, an r^{-2n} relationship is expected. Energy is introduced at the integral scales and flows down the cascade to be eventually removed at the Kolmogorov scale by viscous dissipation. According to Kolmogorov theory, the rate at which energy is produced by Reynolds stresses is identical to the rate at which it is dissipated by viscous stresses [6], implying that it is also identical to the energy flux down the cascade.

At a given Reynolds number, the energy density increases with wave number k until it reaches a peak value at the integral scale [7]. Subsequently, the energy density diminishes monotonically as the wave number increases. As described in [8] this energy is finally dissipated by viscosity. Hence, the total energy E of vortices of size k should depend on the dissipation rate ε, k, and kinematic viscosity ν

$$\frac{E(k)}{\nu^{5/4}\varepsilon^{1/4}} = \frac{E(k)}{v^2\eta} = f(k,\eta) \tag{1}$$

Here, η is the Kolmogorov scale defined as $\eta=(\nu^3/\varepsilon)^{1/4}$ and v is the Kolmogorov velocity defined as $v=(\nu\varepsilon)^{1/4}$.

The centerline energy dissipation rate for axisymmetric jets is given by $\varepsilon=0.5u_c^3/(z-z_0)$ [2], where u_c is the centerline velocity, and $(z-z_0)$ is the downstream distance from the virtual origin of the jet. The integral scale for turbulent jets is of the order of the local jet width b, given by the $1/e$ point of the Gaussian profile approximation to the time-averaged streamwise velocity in a jet. (For the purpose of our study, it is adequate to assume that the integral scale is equal to b.) Substituting for ε in the expression for η, we obtain

$$\eta = \left(\frac{\nu^3(z-z_0)}{0.5u_c^3}\right)^{1/4} \tag{2}$$

Noting also that for an axisymmetric jet, Re based on nozzle diameter (d) and nozzle exit velocity (u_o) is $\approx 1.7bu_c/\nu$, we can write

$$\frac{\eta}{b} = 3\left(\frac{1}{\mathrm{Re}}\right)^{3/4} \tag{3}$$

These expressions are useful for designing the jet experiment and selecting operating parameters as described next. We also describe the details of the vortex eduction tool whereby 2D vector maps obtained using PIV are high-pass filtered to extract their

[1]College of Marine Studies, University of Delaware.
[2]Corresponding author.

Contributed by the Fluids Engineering Division of ASME for publication in the JOURNAL OF FLUIDS ENGINEERING. Manuscript received September 10, 2004; final manuscript received October 25, 2005. Review conducted by Joseph Katz.

 Copyright © 2006 by ASME

Downloaded 06 Feb 2012 to 128.175.188.76. Redistribution subject to ASME license or copyright; see http://www.asme.org/terms/Terms_Use.cfm

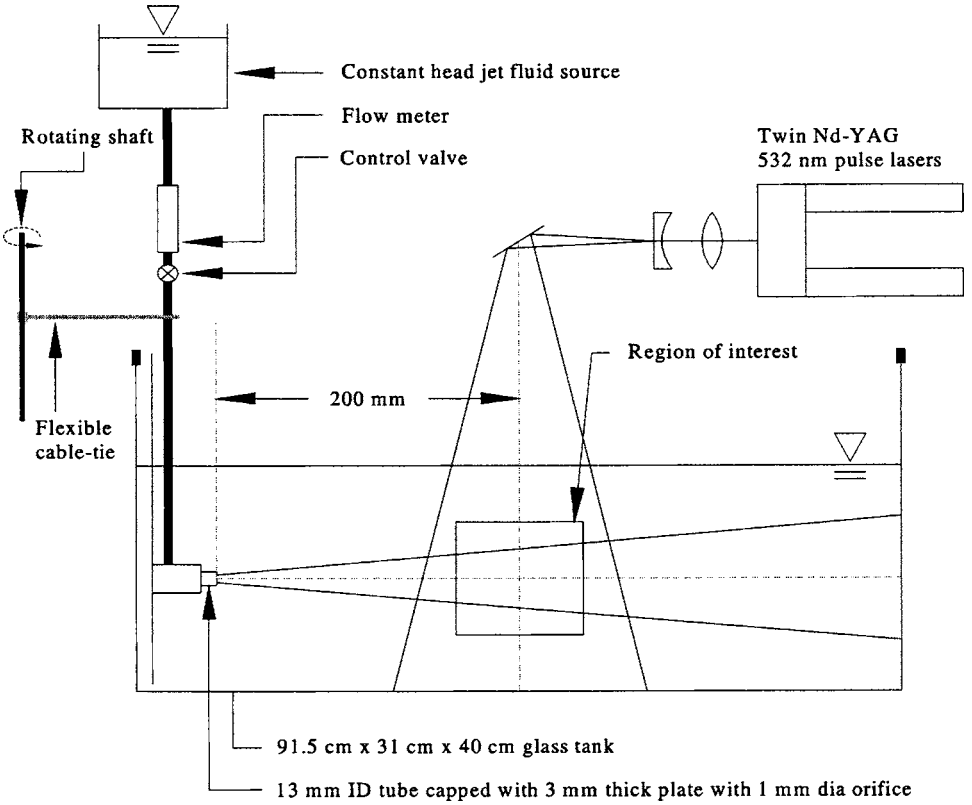

Fig. 1 Schematic of experimental setup

high-frequency content in the form of vortices. Vortex populations, vorticity, and energy distributions are examined and compared to results available in the literature.

Experimental Setup and Measurement Techniques

PIV measurements were conducted in a rectangular glass tank 91.5 cm×31 cm×40 cm high, housing a jet-nozzle assembly mounted to one side of the tank, as shown in Fig. 1. The nozzle assembly consisted of a cylinder (13 mm ID and 46 mm long) capped by a 3 mm thick end plate; a 1 mm dia hole drilled at the center of the end plate served as the jet orifice. One of the challenges in this study was to ensure that the jet remained turbulent even at Reynolds numbers as low as 140. This was achieved by applying a periodic perturbation on the jet supply tubing as will be described shortly. Our nozzle was specifically designed such that this perturbation was not damped by the time the jet emerged from the orifice. The nozzle-cylinder was connected via flexible tubing, a valve, and rotameter to a constant head fluid source mounted on an adjustable height platform. The flow rate and, hence, the Reynolds number for the jet were controlled by adjusting the height of the platform and the valve opening. During experiments, the height of host fluid in the glass tank was equal to the tank width (31 cm), and the nozzle was positioned at the center of this square cross section at one end of the tank, as shown in Fig. 1. The dimensions of the tank relative to the jet nozzle diameter were comparable to previous jet experiments conducted in our laboratory [3–5] and ensured that the finiteness of the host fluid did not influence jet development in any measurable way. Deionized water was used as the working fluid for both the jet and the host. Both fluids were seeded with fluorescent PIV tracer particles (40 μm).

As shown in Fig. 1, PIV measurements were conducted in an axial plane of the jet over a region of interest centered 200 mm downstream from the nozzle. The region of interest was illuminated by twin Nd-YAG lasers (*Continuum* Surelite II) and providing 30 mJ per pulse at a wavelength of 532 nm. The laser beams were passed through a sheet-forming module and steering optics to produce a 1 mm thick vertical laser sheet that was directed downward into the tank through the top surface as shown in Fig. 1. A 10-bit *LaVision* Imager Intense PIV/LIF (laser-induced fluorescence) camera, with a 1376×1040 pixel array was oriented orthogonal to the illuminated plane. The camera magnification was set to capture a width of the jet corresponding to approximately ±1.5b about the jet axis. The view field was set to 140 mm wide for all measurements. A long-wave pass filter was mounted on to the camera lens during PIV measurements to block elastic scattering of laser light while allowing fluorescence to pass through and improve the overall signal quality.

The time separation between laser pulses (4–10 ms, depending on the operating Reynolds number) was chosen to maximize in-plane particle displacement (reducing random error) while still restricting out-of-plane particle motion to acceptable levels. Double-frame images were acquired at 0.5 Hz. The Reynolds number was varied from 140 to 2600. An ensemble of 200 instantaneous velocity fields was acquired for each Reynolds number to compute vortex statistics.

To ensure turbulent flow for even small Reynolds numbers, the jet was tripped by applying a periodic disturbance (4–15 Hz, based on the operating Reynolds number) in the following manner. A flexible nylon self-locking cable tie (Gardner Bender, Part No. 46-108, 20 cm long×2.5 mm wide×0.8 mm thick) was attached to the shaft of a variable speed motor. The cable tie was trimmed to a final length of 15 cm and positioned to impact the flexible jet supply tubing approximately 18 cm (i.e., 180 nozzle diameters) upstream of the nozzle. The low level of the applied forcing and its distance from the nozzle made it far less dominant compared to other jet forcing methods, such as [9] who describe radically altered jets produced by axial and circumferential excitations applied *directly* at the nozzle exit. Furthermore, the Strouhal number ($St=fd/u_o$) of the applied forcing in our experiments

Downloaded 06 Feb 2012 to 128.175.188.76. Redistribution subject to ASME license or copyright; see http://www.asme.org/terms/Terms_Use.cfm

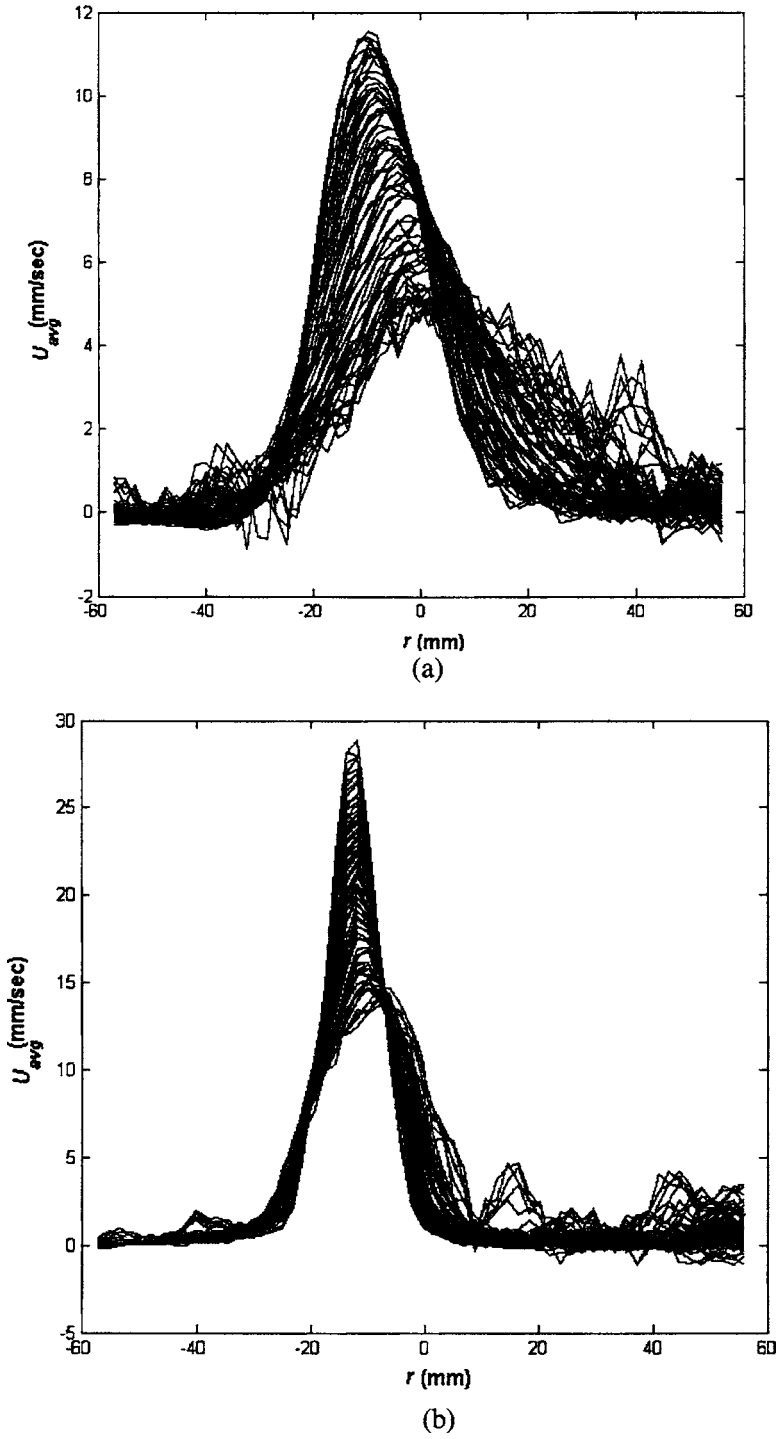

Fig. 2 Time-averaged streamwise velocity profiles for Re=250: (*a*) perturbation turned on (turbulent jet) and (*b*) perturbation turned off (laminar jet)

was in the range of 0.005–0.03, which is one to two orders of magnitude smaller than the "preferred frequency" required to radically alter jet behavior [9].

In our experiments, the revolutions per minute (rpm) of the variable speed motor and, hence, the frequency of the applied disturbance was selected after careful visual evaluation of the jet behavior. A small amount of sodium hydroxide and thymolphthalein (an indicator that turns blue for pH$\geqslant$8.5 and is colorless otherwise) was added to the jet supply reservoir to visualize the jet emerging into the host fluid and confirm that the jet remained turbulent even at the smallest Reynolds numbers employed in this study. When the jet fluid underwent turbulent mixing with the host, its pH dropped below the threshold value rendering it colorless. The use of this pH-indicator method allowed an effective visualization of the turbulent nature of the emerging jet even during a PIV run, without incurring a buildup of dye in the tank that would impair PIV recording.

In addition to visual evaluation of the jet, time-averaged axial velocity profiles were plotted at various downstream locations for all the Reynolds numbers used in the study. Figure 2 shows two dramatically different plots for U_{avg} for Re=250. The first plot corresponds to the turbulent jet (perturbation has been turned on),

Downloaded 06 Feb 2012 to 128.175.188.76. Redistribution subject to ASME license or copyright; see http://www.asme.org/terms/Terms_Use.cfm

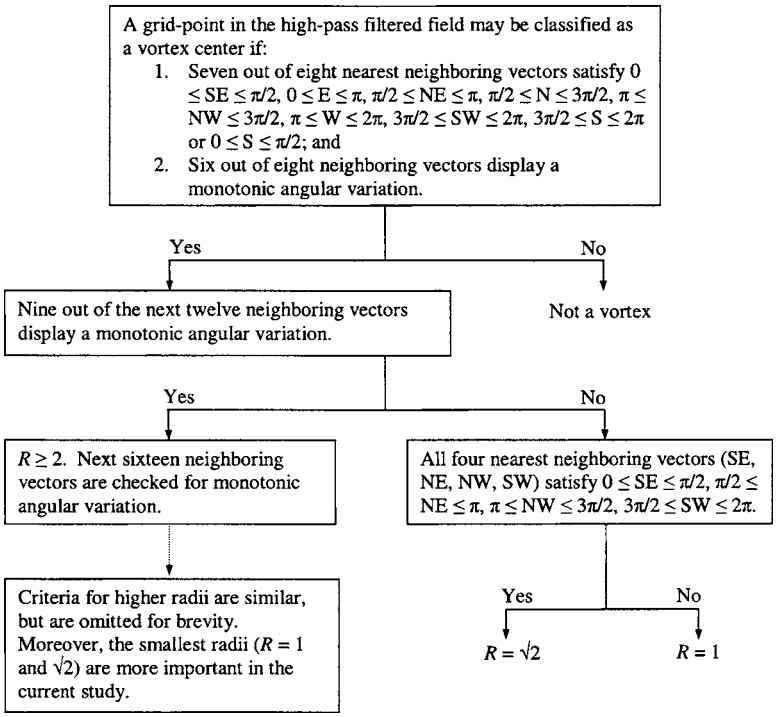

Fig. 3 Flow chart for identifying a vortex center and determining its radius

and the second plot corresponds to the laminar jet (perturbation is off). The centerline velocity is substantially smaller for the turbulent case (10 mm/s max) relative to the laminar case (25 mm/s max), which is the expected behavior. The laminar jet is also very narrow due to minimal mixing with the ambient fluid. On the other hand, the turbulent jet displays the typical rapid mixing with the ambient fluid and spreads laterally at the typical rate for turbulent jets. As an aside, note that both the turbulent and laminar jets lean slightly to the right as they proceed downstream (which actually means downward in the experimental situation because the jet is horizontally directed from left to right). This is because it is difficult to accurately match the jet density to the host density and the effect is more pronounced at low Re. However, since our vortex eduction technique uses the high-pass filtered velocity field, this slight tilt has a negligible effect on the vortex statistics that are of interest in this paper.

The velocity profile for even the smallest Reynolds number resembled those for higher Reynolds numbers. Furthermore, the two characteristic constants for turbulent jets (the centerline velocity decay constant B_u and the jet spread rate c) were calculated for all Re used in the study and found to be close to values commonly quoted in the literature (B_u=5.7, c=0.1) for turbulent jets. Finally, rms profiles for all Re were plotted for each downstream distance. Turbulent jet literature quotes the ratio of the rms to the mean velocity at about 0.25 at the centerline. Our rms results provide a value that is very close to that expected for turbulent jets.

Cross correlation, with double-pass grid refinement was used for PIV processing, resulting in a final interrogation spot size of 32×32 pixels with 50% overlap. The resolution of the square grid of the resulting vector fields was 1.63 mm. The particle displacement measurement error is about 0.1 pixels, which corresponds to a relative error in the velocity measurement of about 1–2% at the centerline.

Vortex Education Technique

A high-pass filtering technique [3,10] was used for educing vortices that were identified using the definition provided by [11]. First, the instantaneous velocity field is smoothed using a Gaussian kernel. The resulting field is thus low-pass filtered. Next, the high-pass filtered field is obtained by subtracting the low-pass filtered field from the instantaneous field, exposing the vortices. The standard deviation of the smoothing Gaussian kernel was set to three grid units, and the filter was truncated at five grid units [5]. An automated method was employed for counting the number of vortices as described in [5]. Briefly, a point in the high-pass filtered field was identified as a vortex center if the neighboring vectors displayed a monotonic variation in angular orientation from 0 to 2π while moving in a closed path around it; specific details for the identification of the smallest radii (1 and $\sqrt{2}$) are presented in Fig. 3. Details for higher radii are similar, but are omitted for brevity and also because the smallest radii are the focus of the current study. The robustness of the education technique can be confirmed by the good comparison between the educed vortices and the corresponding standard vorticity plot (see Fig. 5, Ref. [4]). In addition to the algorithm described in [5] and in Fig. 3, it was also necessary to employ one additional criterion in the present work. At low Reynolds numbers, the magnitude of the vectors in the high-pass filtered field falls to <0.1 pixels, which is comparable to the error in the PIV measurement. In order to circumvent the detection of spurious vortices from such vector fields, we set a threshold value for the average velocity magnitude within a vortex of 0.07 pixels, in order to accept a vortex as a valid one. Our automated code identifies vortices of sizes 1, $\sqrt{2}$, 2, $\sqrt{5}$, $\sqrt{8}$, 3, 10, and $\sqrt{13}$ grid units (each radius value is the square root of the sum of the squares of two integers). The outermost radial position that passed the check mentioned in Fig. 3 was marked as the radius R of that vortex. Vortex radius (R), rotational sense (clockwise or counterclockwise), and circulation (Γ) were measured directly, and energy (E) and vorticity (ω) were derived. Circulation is defined as

$$\Gamma = \oint u' \cdot ds \tag{4}$$

where u' is the high-pass filtered velocity vector. Energy density is calculated as

Downloaded 06 Feb 2012 to 128.175.188.76. Redistribution subject to ASME license or copyright; see http://www.asme.org/terms/Terms_Use.cfm

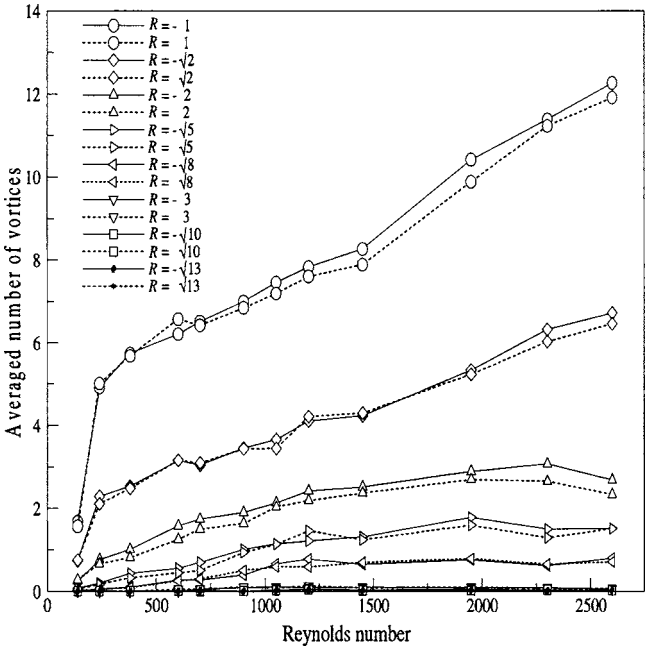

Fig. 4 Variation of number of vortices (per frame) with Reynolds number. Negative radius values in the legend correspond to clockwise eddies.

$$E(k) = \frac{c_1 \Gamma^2}{k} \tag{5}$$

where k is the wave number and c_1 is a constant. (We have set $c_1 = 1$ for the energy plots presented in this paper.) Vorticity is calculated as

$$\omega = \frac{\Gamma}{R^2} \tag{6}$$

Results and Discussions

The vortex education tool described earlier (Fig. 3) was used to explore the variation of vortex populations for various Re and vortex radius R. In Fig. 4, we plot vortex populations sorted by vortex radius against Re. The plot contains three important results: (i) The vortex populations for clockwise[3] and counterclockwise eddies are almost identical, which is expected from symmetry considerations and thus lends confidence to our eduction tool; (ii) For a given Re, the vortex population decreases continuously with increasing radius, which is consistent with the space-filling hypothesis (we will explore this aspect in greater detail shortly); and (iii) For a given vortex radius, the vortex population decreases monotonically as Re is decreased (especially for vortices of smaller radii), with a precipitous drop in population at the smallest Re of 140. The dramatic decay in number of vortices of small radii ($R = \pm 1, \pm\sqrt{2}$) below Re=250 indicates that these eddies are approaching the Kolmogorov scale, beyond which viscosity suppresses eddy formation. Equation (3) indicates that $\eta \approx 1.47$ mm (see also Table 1) for Re=140 at a midframe downstream distance of $200d$, which compares well with the smallest vortex size in Fig. 4. The number of vortices for larger radii also decreases for Re <250, but the change is not as significant as it is for smaller radii.

Figure 5 is simply a rearrangement of the data in Fig. 4, in that we now plot vortex populations sorted by Re against vortex radius. The vortex population (N) and the vortex radius (R) are normalized by their corresponding values for $R=1$, respectively.

[3]Clockwise eddies are denoted by negative radius values in the legend in Fig. 4.

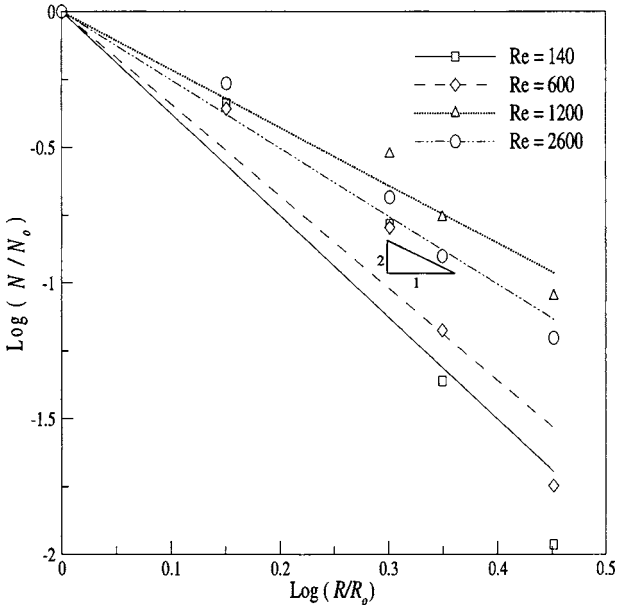

Fig. 5 Linear fits for ratio of vortex population and radius

Table 1 Kolmogorov scale at the centerline of round jets at $z/d=200$ for different Reynolds numbers

Reynolds number	Kolmogorov scale (mm)
140	1.47
240	1
380	0.7
600	0.49
700	0.43
900	0.37
1050	0.33
1200	0.29
1450	0.26
1950	0.21
2300	0.18
2600	0.16

The experimental data (for $R<3$) are reasonably fit by straight lines with slopes ranging from −2.1 for Re=1200 to −3.7 for the lowest Re of 140. Large vortices are sparse at low Re, and therefore, there is a greater sampling error associated with their populations.[4] Consequently, we focus on the data for Re=1200 (slope=−2.1) and 2600 (slope=−2.5) in Fig. 5. Both their slopes are close to −2. This result appears to be in accord with the space-filling argument, in that the vortex population in a two-dimensional domain should grow as R^{-2} when moving from one vortex size to the next.

Kinetic energy of the vortices of different size is plotted in Figs. 6 and 7. Essentially, the energy density curve reaches a maximum at a wave number corresponding to the integral scale and decreases for higher wave numbers. The energy density plot in Fig. 6 was obtained as follows. First, we summed the total energy contained by all vortices of a given radius in the entire record. Next, we divided this total by the number of frames to get the average energy for that vortex radius per frame; the average en-

[4]It should be noted that slopes of the Re=140 and 600 lines are close to 2 if vortices of larger radii are ignored.

Downloaded 06 Feb 2012 to 128.175.188.76. Redistribution subject to ASME license or copyright; see http://www.asme.org/terms/Terms_Use.cfm

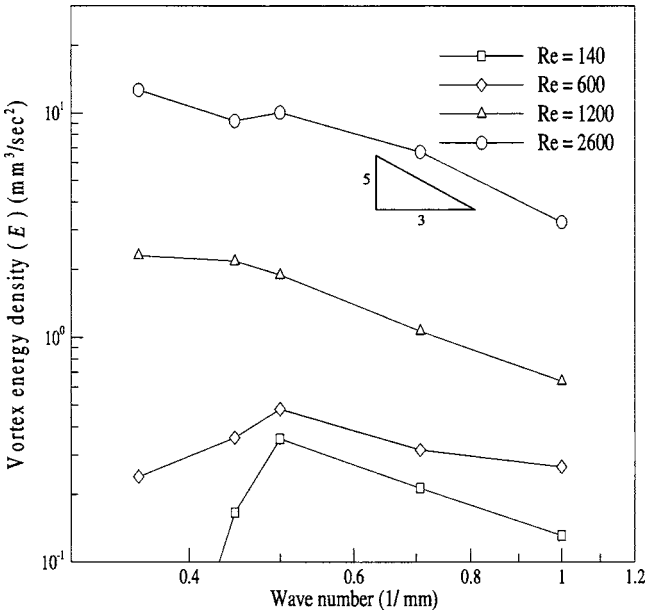

Fig. 6 Variation in vortex energy with vortex size (energy averaged per frame)

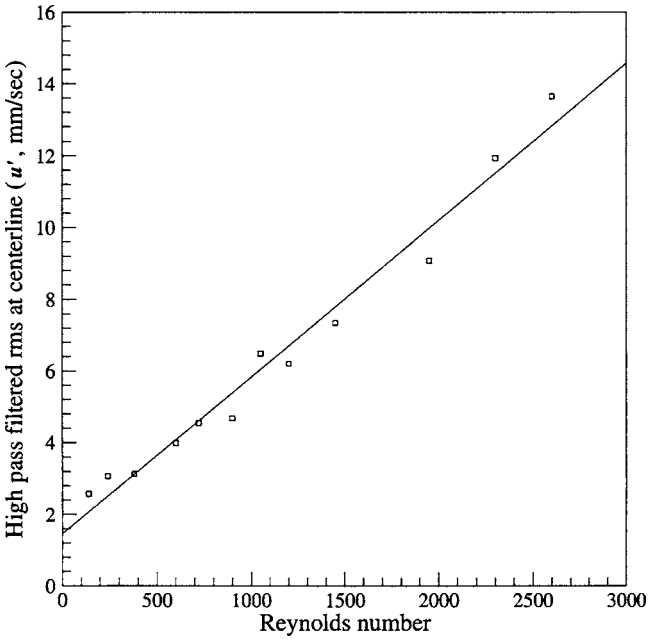

Fig. 8 Variation of centerline rms (u') of high-pass filtered velocity field with Reynolds number

ergy per unit area was then obtained by dividing by the area of the frame. Finally, because the energy of all eddies of size $2\pi/k$ is proportional to $E(k)$ times the width of the energy spectrum, which is k [7], we can obtain $E(k)$ by dividing the average energy per unit area by k. The energy plots shown in Fig. 6 match fairly well with theory that predicts a $E(k)$ versus k slope of $-5/3$ in the inertial subrange. Figure 6 indicates a slope of about -1.3 for the larger Re values. As expected, energy values decrease with Reynolds number for every wave number. Figure 7 presents the energy data of Fig. 6 in dimensionless form (energy density is normalized by $u_c^2 b$). The energy density curve indicates a reasonably good collapse for wave numbers greater than $0.1b/R$.

Typically in turbulence studies, rms of the velocity signal is measured directly, using a pointwise technique, such as hot-wire anemometry or laser-Doppler anemometry. Here, we extract rms of the high-pass filtered velocity using PIV measurements with good spatial resolution but limited temporal resolution. The rms of the high-pass filtered streamwise velocity (u') at the centerline is plotted against Reynolds number in Fig. 8; the data are fit well by a straight line. A linear relationship is to be expected because all velocities scale with the local centerline velocity u_c, which, in turn, is proportional to Re. Note that the fit to the data does not pass through the origin, suggesting that a small portion of the measured rms may arise from noise in the velocity data. The slope of the line is 0.0044 mm/s. Using the well-known correlation for *total* (i.e., across all wave numbers) rms at the centerline ($u'/u_c = 0.25$, which can be rewritten as $u'/\mathrm{Re} = 0.15\, v/b$), it is readily

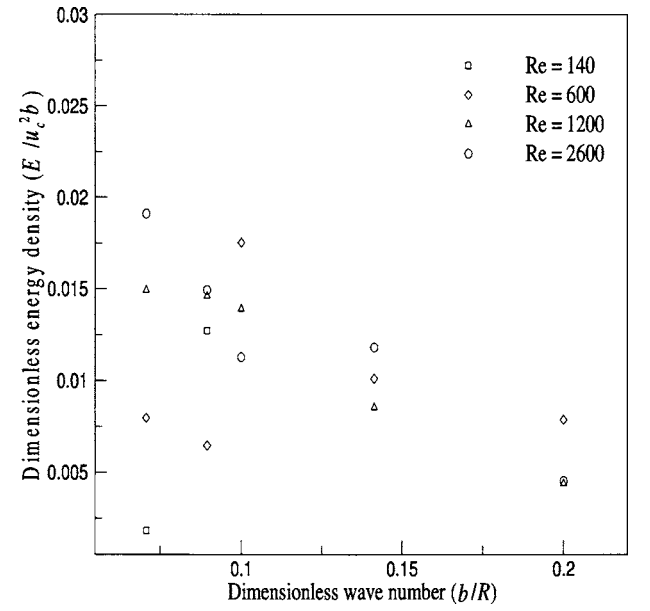

Fig. 7 Variation of nondimensional vortex energy with vortex size

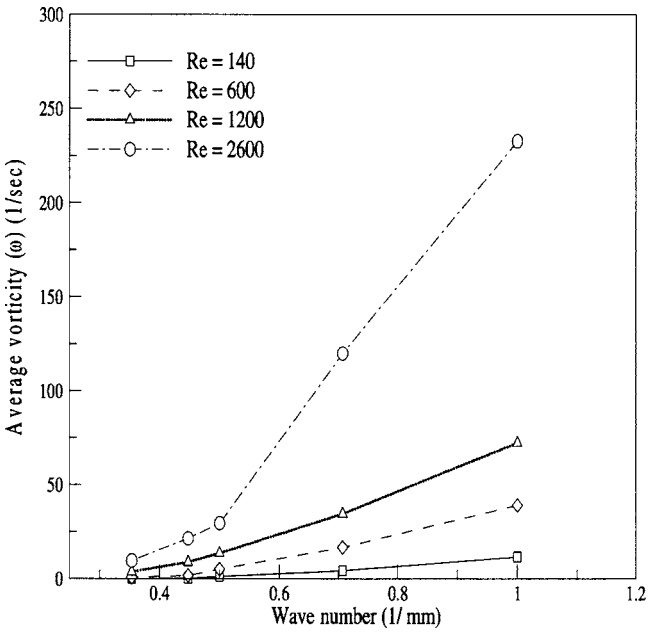

Fig. 9 Variation in average vorticity with vortex size

Downloaded 06 Feb 2012 to 128.175.188.76. Redistribution subject to ASME license or copyright; see http://www.asme.org/terms/Terms_Use.cfm

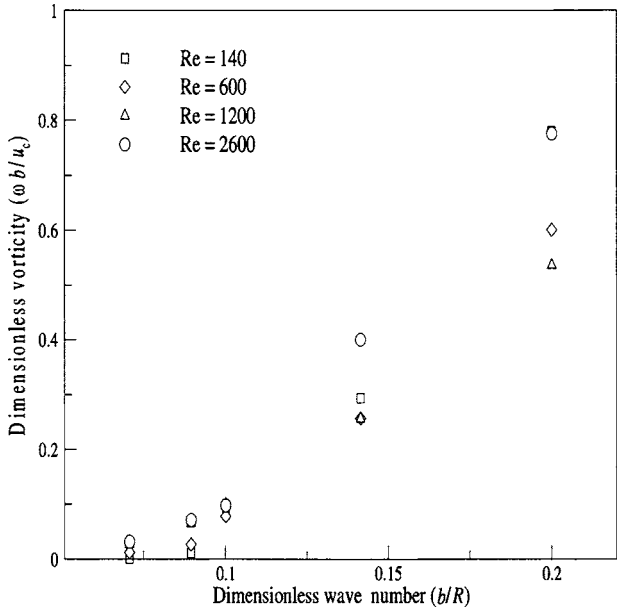

Fig. 10 Variation of nondimensional vorticity with vortex size

shown that the slope of u' versus Reynolds number should be 0.0075 mm/s for our experimental conditions. The difference between the two slopes is contributed by the low-pass field, which carries the remainder of the rms with it. For the size of the filter used in our study, we can conclude that approximately two-thirds of the total rms (or about half the total energy) is carried by the high-pass filtered field.

Vorticity (averaged over 200 frames) sorted by Reynolds number is plotted against vortex size in Figs. 9 and 10. It is evident that vorticity increases with k and that the relative increase in the vorticity is greater for larger Reynolds numbers (Fig. 9). When Fig. 9 is replotted in dimensionless form in Fig. 10, the data collapse quite well and confirm that vorticity increases with wave number.

Conclusions

Characteristics of small vortices in turbulent jets are obtained by applying a vortex education tool to high-pass filtered $2D$ velocity fields. Vortex characteristics are obtained at scales approaching the Kolmogorov scale by employing jets at low Reynolds numbers at which they would ordinarily be laminar. The jets are forced to remain turbulent at these low Re's by applying a periodic perturbation to the jet fluid. Results show that the vortex population drops substantially when the eddy size approaches the Kolmogorov scale. Vortex populations sorted by Reynolds number are consistent with the space-filling argument in two dimensions. The energy density varies with wave number as $-5/3$ for the inertial subrange, and vorticity increases with wave number. For the size of the filter used in our study, approximately two-thirds of the total rms (or about half the total energy) is carried by the high-pass filtered field.

References

[1] George, W. K., and Baker, C. B., 1980, "Analysis of Hot-Wire-Measurements in Turbulent Jets," Bull. Am. Phys. Soc., **25**(9), p. 1074.
[2] Hussein, H. J., Capp, S. P., and George, W. K., 1994, "Velocity Measurements in a High Reynolds Number, Momentum-Conserving Axisymmetric Turbulent Jet," J. Fluids Mech., **258**, pp. 31–75.
[3] Agrawal, A., and Prasad, A. K., 2002, "Properties of Vortices in the Self-Similar Turbulent Jet," Exp. Fluids, **33**, pp. 565–577.
[4] Agrawal, A., and Prasad, A. K., 2003, "Measurements Within Vortex Cores in a Turbulent Jet," ASME J. Fluids Eng., **125**, pp. 561–568.
[5] Agrawal, A., and Prasad, A. K., 2002, "Organizational Modes of Vortices in an Axisymmetric Turbulent Jet," Flow, Turbul. Combust., **68**, pp. 359–377.
[6] Frisch, U., 1995, *Turbulence: The Legacy of A. N. Kolmogorov*, Cambridge University Press, Cambridge, England.
[7] Hinze, J. O., 1959, *Turbulence: An introduction to Its Mechanism and Theory*, McGraw-Hill, New York.
[8] Tennekes, H., and Lumley, J. H., 1972, *A First Course in Turbulence*, The MIT Press, Cambridge, MA.
[9] Reynolds, W. C., Parekh, D. E., Juvet, P. J. D., and Lee, M. J. D., 2003, "Bifurcating and Blooming Jets," Annu. Rev. Fluid Mech., **35**, pp. 295–315.
[10] Adrian, R. J., Christensen, K. T., and Liu, Z.-C., 2000, "Analysis and Interpretation of Instantaneous Turbulent Velocity Fields," Exp. Fluids, **29**, pp. 275–290.
[11] Robinson, S. K., Kline, S. J., and Spalart, P. R., 1989, "Quasi-Coherent Structures in the Turbulent Boundary Layer. Part II: Verification and New Information From a Numerically Simulated Flat-Plate Boundary Layer," *Near Wall Turbulence, Proceedings of Zaric Memorial Conference*, S. J. Kline and N. H. Afgan, eds., Hemisphere, New York, pp. 218–247.

Downloaded 06 Feb 2012 to 128.175.188.76. Redistribution subject to ASME license or copyright; see http://www.asme.org/terms/Terms_Use.cfm